Article

Not peer-reviewed version

Electrochemical Corrosion Behavior of SiO_2 Superhydrophobic as Corrosion Inhibitor in Al7075

Jesús Manuel Jáquez-Muñoz *, Luis Eduardo Vázquez Nuñez, Betania Sánchez-Santamaria, José Saúl Arias-Cerón, Jaime Santana, Abel Diaz Olivearez, Luis Enrique Arambula Miranda, Martha Guadalupe Carrera Rámirez, Aurora Abigail López-Ibarra, Delfino Cornejo Monroy *

Posted Date: 27 August 2025

doi: 10.20944/preprints202508.1927.v1

Keywords: superhydrophobic; SiO_2 coating; aluminum; electrochemical impedance spectroscopy (EIS) and inhibitor

 doi:10.20944/preprints202508.1927.v1

Article

Electrochemical Corrosion Behavior of SiO_2 Superhydrophobic as Corrosion Inhibitor in Al7075

Jesús Manuel Jáquez-Muñoz [1,*], Luis Eduardo Vázquez Nuñez [2], Betania Sánchez-Santamaria [1], José Saúl Arias-Cerón [3], Jaime Santana [1], Abel Diaz Olivarez [1], Luis Enrique Arambula Miranda [1], Martha Guadalupe Carrera Rámirez [2], Aurora Abiagil López-Ibarra [2] and Delfino Cornejo Monroy [2,*]

[1] Universidad Autónoma de Aguascalientes, Centro de Ciencias de la Ingeniería, Aguascalientes 20340, Mexico

[2] Universidad Autónoma de Ciudad Juárez, Instituto de Ingeniería y Tecnología

[3] Universidad Popular Autónoma del Estado de Puebla

* Correspondence: jesus.jaquez@edu.uaa.mx (J.M.J.-M.); delfino.cornejo@uacj.mx (D.C.M.)

Abstract

Automotive industry has been employed Al alloys to reduce weight of chassis, however it can present some corrosion problems. In this research we study the electrochemical behavior of SiO_2 superhydrophobic on Al 7075. The electrochemical techniques employed were cyclic potentiodynamic polarization (CPP) taken 60 mV/m from -800 to 800 mV vs. OCP and electrochemical impedance spectroscopy (EIS) at ± 10 mV at 10 mHz to 100 kHz based on ASTM G61 and ASTM G106. The electrolytes employed where NaCl and H_2SO_4 at 3.5 wt.% simulating marine and industrial atmospheras. The results showed that coating presented a efficiency of 81% when is exposed to NaCl, but the corrosion presented in this media is localized; in H_2SO_4 the corrosion type is uniform.

Keywords: superhydrophobic; SiO_2 coating; aluminum; electrochemical impedance spectroscopy (EIS) and inhibitor

1. Introduction

Nowadays, the automotive industry is interested in reducing the weight of vehicles by employing materials such as aluminum alloys, advanced high-strength steels, magnesium, and composites. The use of Al alloys in the automotive industry has increased in recent years; however, those materials are susceptible to present corrosion problems [1].

Al alloys employed in the automotive industry are the series 7XXX, 6XXX, and 5XXX. These alloys are available in sheets or by extrusion. Nissan has significantly reduced its use of Al alloys and AHSS in the BIW of the vehicle. However, those alloys are exposed to corrosion problems due to the environment in which they are employed [1–3].

The cause of corrosion can be related to environmental factors, such as the presence of oxygen in water and salt, which can promote the process. Salts often serve as electron carriers, enabling water to transport them through redox reactions. In humid environments, metals corrode significantly faster. This happens because moisture-laden air interacts with oxygen and electrons on the metal's surface. Prolonged exposure to humid air accelerates the corrosion of metal components. Vehicles encounter diverse environmental conditions, ranging from extreme heat and cold to operation in coastal regions or near chemical plants. These factors all play a role in atmospheric corrosion. Even a small scratch during use can create a corrosion cell within the surface's moisture film, while the application of de-icing salts in cold climates can accelerate the process [4].

One option to prevent corrosion problems in the automotive industry is the application of coatings that reduce the interaction between metal and the environment. There are various methods

 doi:10.20944/preprints202508.1927.v1

to protect materials from corrosion, including anodization, vapor deposition, chemical conversion, plasma spraying, and organic coatings. Inhibitors, which can be part of both organic and inorganic coatings, primarily serve to slow down the corrosion process. Their effectiveness is closely linked to their adsorption capacity; however, factors such as inhibitor properties, electrolyte concentration, and changes in surface charge can influence the adsorption performance of the inhibitor [5–11].

Silicon dioxide (SiO_2), an inorganic nanoparticle, is commonly used to improve the performance of various organic-based resins. Its strong mechanical and thermal properties make it an effective barrier material. Additionally, numerous studies have demonstrated that SiO_2 exhibits hydrophobic characteristics, which help block corrosive agents from interacting with the surface and prevent the penetration of corrosive ions [16]. Superhydrophobic surfaces, known for their water-repellent behavior, are considered highly effective in corrosion protection. They are defined by a static water contact angle greater than 150° and a tilt angle below 10° [12–17].

Research has shown that SiO_2 coatings can lower the corrosion rate by altering surface porosity, and corrosion resistance is further enhanced when SiO_2 is combined with epoxy resins. Various corrosion inhibitors have also been developed based on the hydrophobic properties of coatings. A reduction in corrosion kinetics occurs with a hydrophobic coating in NaCl at 3.5 wt.% [18]. Superhydrophobic surfaces are particularly useful in anodized materials, as they help reduce Cl^- ion penetration due to anodized porosity. These surfaces offer solutions to corrosion issues caused by environmental pollutants. The role of hierarchical structures in superhydrophobic surfaces is based on the contact angle of 160° and a sliding angle of 1°, enabling a self-cleaning effect [19–21]. Localized corrosion, such as intergranular corrosion, can significantly reduce the service life of materials like the AA7075 aluminum alloy. The alloy's microstructure—determined by the heat treatments applied—plays a key role in influencing its susceptibility to localized corrosion. However, the relationship between microstructure and localized corrosion behavior remains not fully understood, with varying interpretations in the literature. For instance, the T6 aging process has been associated with a heightened risk of intergranular corrosion (IGC) [22–24]. Xiong et al. [25] found that applying different heat treatments to Al-7075 resulted in distinct localized corrosion patterns, influenced by the anodic nature of the affected areas. Their research also suggests that the GL test, which is faster, avoids the need for complex test-time selection, and yields cleaner specimen surfaces, may be a more efficient method for predicting localized corrosion behavior under natural conditions—without the need for an applied current—compared to the OCP test.

Some researchers showed that when superhydrophobic is applied on the surface, the Ecorr value increases 0.1 V vs. SCE, meaning that the potential is more noble. The current values are decreasing by three orders of magnitude, indicating that corrosion kinetics is lower when the coating is applied, which is characterized by potentiodynamic polarization [21,26–28].

When EIS was conducted, the results showed that the n values are close to 1, indicating the presence of some porosity, but with a trend to be homogenous. However, the inhibition efficiency is nearly 100%, indicating that the corrosion resistance is higher and the material is protected against corrosion [29,30].

This work aims to evaluate the electrochemical corrosion behavior of Al7075 coating with a superhydrophobic coating of Si_2O nanoparticles. The electrochemical techniques employed to realize this study are cyclic potentiodynamic polarization (CPP) and electrochemical impedance spectroscopy in the electrolytes of NaCl and H_2SO_4 at 3.5wt.% to simulate marine and industrial environments based on ASTM G106 and G61.

2. Materials and Methods

2.1. Materials

Silica nanoparticles (SiO_2 NPs) were prepared using tetraethyl orthosilicate (TEOS, 98%, Sigma-Aldrich) as the precursor, with ammonium hydroxide (28–30% NH_3, Sigma-Aldrich) serving as the catalyst. Deionized water (18 MΩ·cm) and isopropyl alcohol (C_3H_8O, CEDROSA) were used as

 doi:10.20944/preprints202508.1927.v1

solvents during hydrolysis. For surface modification and formation of a superhydrophobic layer, hexane (95%, J.T. Baker) and 1H,1H,2H,2H-perfluorodecyltriethoxysilane (PFDTES, 97%, Matrix Scientific) were employed. Glass slides for coating experiments were obtained from Fisher Scientific.

2.2. Equipment

A water purification unit (Water-Pro PS, Labconco®) provided the deionized water. Solution mixing was performed using a magnetic stirrer (PC 410, Corning®), and the resulting coatings were examined with a scanning electron microscope (JSM-7401, JEOL).

2.3. Synthesis and Coating Procedure

SiO_2 nanoparticles were synthesized following the Stöber method. A mixture of 95 mL isopropyl alcohol was stirred at 300 rpm, then 350 µL ammonium hydroxide, 1 mL TEOS, and 3.65 mL deionized water were added. The reaction proceeded at 40 °C for 24 hours under continuous stirring. Subsequently, 500 µL PFDTES and 25 mL hexane were incorporated, and the temperature was raised to 60 °C. Stirring continued for 48 hours, yielding 125 mL of the superhydrophobic solution.

Glass substrates were coated using a spray method, applying 1, 3, 5, or 7 layers. The nozzle was positioned 15 cm from the surface, with an air pressure of 30 psi. After coating, the samples were exposed to outdoor conditions for 35 days to evaluate the stability of their superhydrophobic properties.

2.4. Electrochemical characterization

A three-electrode setup (Figure 3) was employed to study corrosion, where the test material acted as the working electrode, a saturated calomel electrode (SCE) served as the reference, and a platinum wire functioned as the counter electrode. All measurements were repeated twice at ambient temperature using a Princeton Applied Research Model 263A (UK). The experiments were conducted in a 3.5 wt.% NaCl and H_2SO_4 aqueous solution. Cyclic potentiodynamic polarization was performed based on ASTM G61-86. One cycle was used in a polarization range of -0.8 to +0.8 V relative to E_{corr} with a 60 mV/min sweep rate [31]. The electrochemical impedance spectroscopy (EIS) was performed based on ASTM G106, with a frequency range of 0.01 Hz to 100 kHz, an applied signal amplitude of 10 mV RMS, and 35 measurement points per decade. EIS data were analyzed through **ZView-4** software (Scribner Associates, Inc., Southern Pines, NC, USA), using equivalent circuit modeling to interpret the spectra.

3. Results

3.1. SEM Before Corrosion

Figure 1 shows the morphology of Al 7075 at SEM before and after the application of SiO_2 hydrophobic. Figure 1a-b shows the Al 7075, which presents some porosity and the lines due to the grind. Besides, Figure 1c-d shows the coating; the inhibitor does not present a homogeneous distribution, presenting zones with cracks that resemble dry earth.

 doi:10.20944/preprints202508.1927.v1

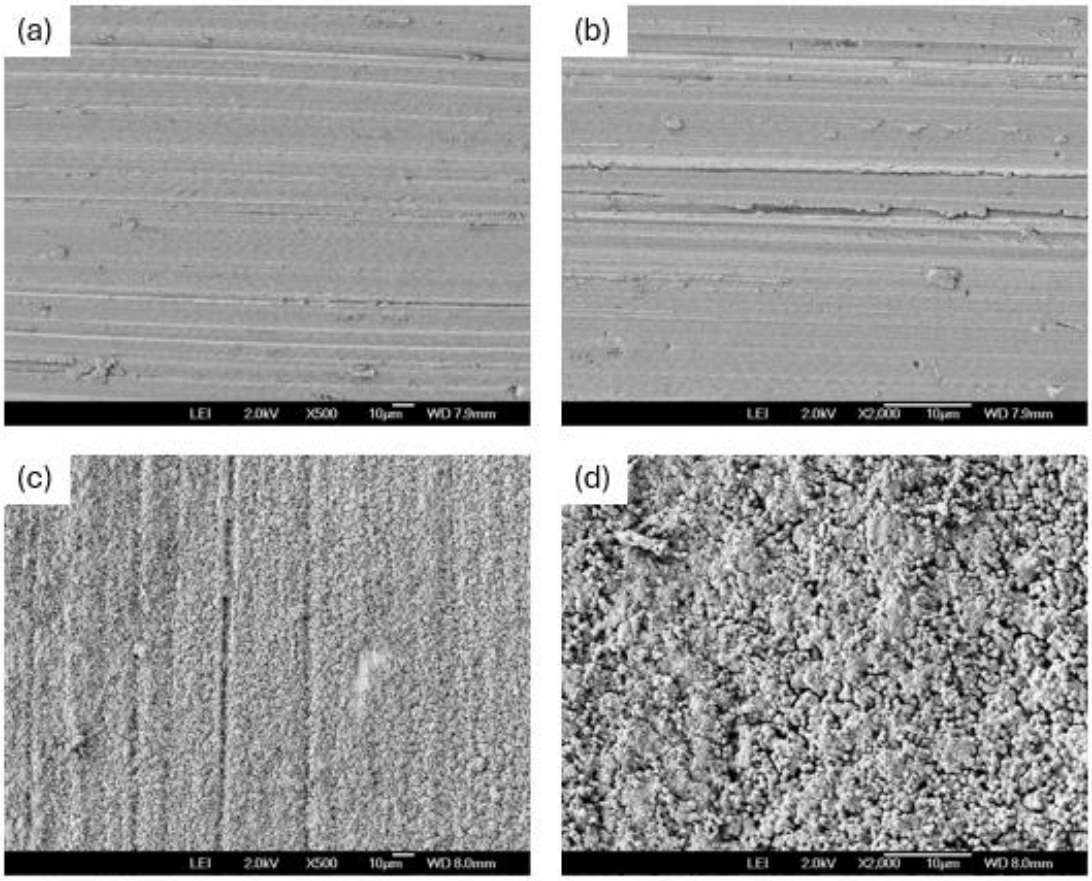

Figure 1. SEM analysis. SEM analysis. (a) Al-7075 at 500X, (b) Al-7075 at 2000X, (c) Al 7075 coated with SiO_2 inhibitor at 500X, and (d) Al 7075 coated SiO_2 inhibitor at 2000X before corrosion test.

3.2. Wettability Test

Figure 2 presents the wettability results, showing a water contact angle (WCA) of 157.5° ± 1.18° and a water sliding angle (WSA) of 3.2° ± 0.29°. These values confirm that the coating retains its superhydrophobic behavior.

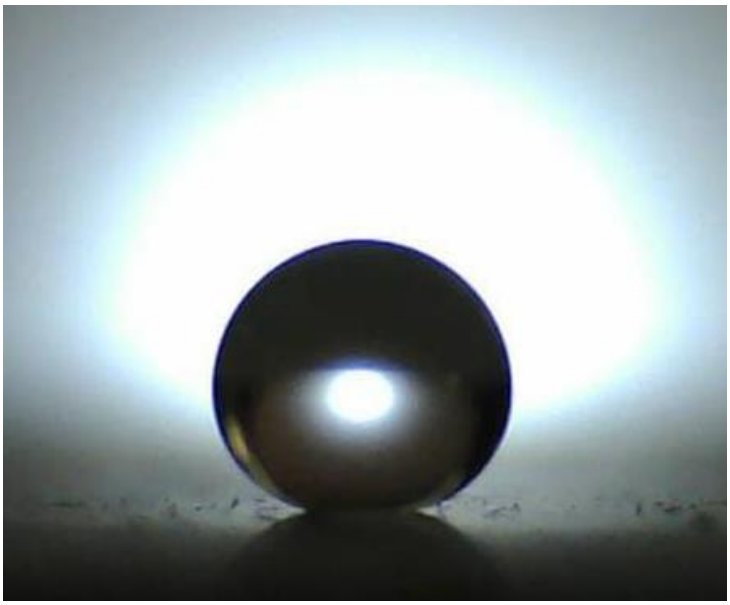

Figure 2. Image of water droplet on glass substrate.

 doi:10.20944/preprints202508.1927.v1

3.3. Electrochemical Test

3.3.1. Cyclic Potentiodynamic Polarization

Figure 3 shows the CPP of samples when they are exposed to NaCl and H_2SO_4. Figure 3(a) shows the behavior of samples when they are exposed to NaCl. The uncoated Al 7075 sample presents a lower Ecorr, -750 mV, and the coated sample presents a value of -721 mV (See table 1). The increase in E_{corr} indicates that the coated sample has a higher corrosion potential, and the corrosion probability decreases. The i_{corr} is lower for Al 7075 SiO_2 (5.91×10^{-5} A/cm²), indicating a lower corrosion rate compared to the 1.54×10-4 A/cm2 of Al 7075, which presents a higher corrosion rate. The samples presented positive hysteresis, indicating a localized corrosion in both samples.

Figure 3(b) shows the results of samples when they are exposed to H_2SO_4. The sample Al 7075 SiO_2 obtained an E_{corr} of -420 mV and Al 7075 -589 mV, indicating that the coated sample requires more energy to initiate an anodic process. The i_{corr} of Al 7075 SiO_2 is 2.28×10-4 A/cm2, while Al 7075 presented 1.45×10-3 A/cm2, indicating that the corrosion rate increases when the sample is uncoated. The samples presented uniform corrosion due to the positive hysteresis.

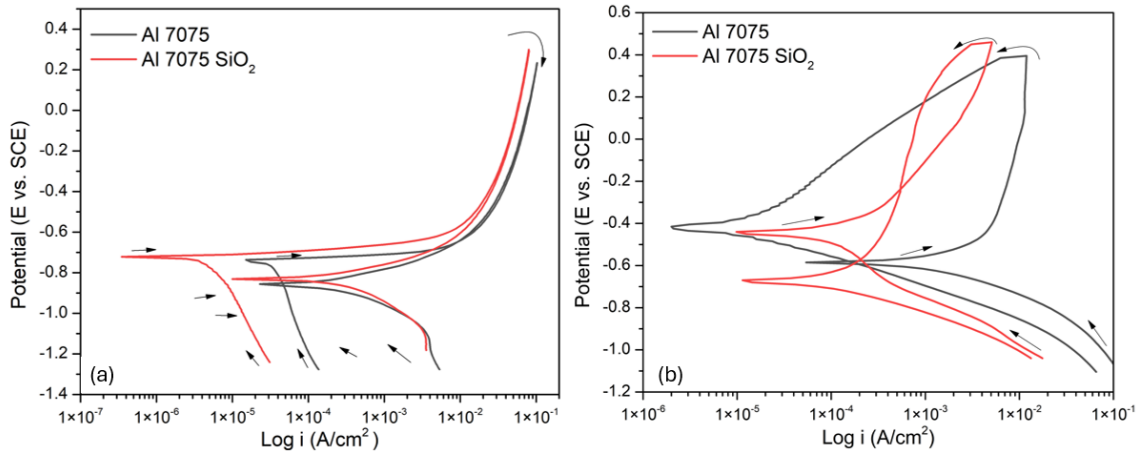

Figure 3. CPP of Al 7075 and Al 7075 coated by SiO_2 when is exposed to (a) NaCl and (b) H_2SO_4.

Table 1. CPP parameters obtained by experimentation.

Sample	E_{corr} (mV)	i_{corr} (A/cm²)	Hysteresys
NaCl			
Al 7075	-750	1.54×10^{-4}	Positive
Al 7075 SiO_2	-721	5.91×10^{-5}	Positive
H_2SO_4			
Al 7075	-589	1.45×10^{-3}	Negative
Al 7075 SiO_2	-420	2.28×10^{-4}	Negative

3.3.1. Electrochemical Impedance Spectroscopy

Figure 4 shows the results of EIS for samples exposed to NaCl. The value of CPE is higher for Al 7075 SiO_2 with a value of 6.6×10^{-5} F/cm² (see Table 2), indicating a high ionic energy. The n value of Al 7075 is 0.68, suggesting a non-homogeneous current distribution on the surface, which may be due to a localized process. On the other hand, the value of Al 7075 SiO_2 is 0.9036, indicating that the surface is nearly homogeneous, but is not perfect. It's main that corrosion will be attacked in preference zones. The second layer presented negative values of n, indicating that the CPE has an inductor behavior. This means that an adsorption process is occurring on the surface. Figure 4(b)

 doi:10.20944/preprints202508.1927.v1

shows the absolute impedance vs. frequency. This graphic indicates that Al 7075 SiO2 presented a higher corrosion resistance; therefore, the efficiency of inhibitors (IE) is higher, with values of 81.37%. The IE is calculated with the following equation [32]:

$$IE = \frac{(R_T - R_{TC})}{R_T} \times 100 \qquad (1)$$

Where:

$$R_T = R_{ct} + R_C \qquad (2)$$

The inhibitor increased the corrosion resistance; therefore, the efficiency is higher. The Bode phase angle diagram shows how the adsorption behavior begins to occur at low frequencies, around 1×10^{-1} Hz, and that behavior occurs in the second layer, when the electrolyte penetrates the material. For that reason, although the inhibitor protects Al 7075 from corrosion, it cannot change the mechanism of corrosion of aluminum.

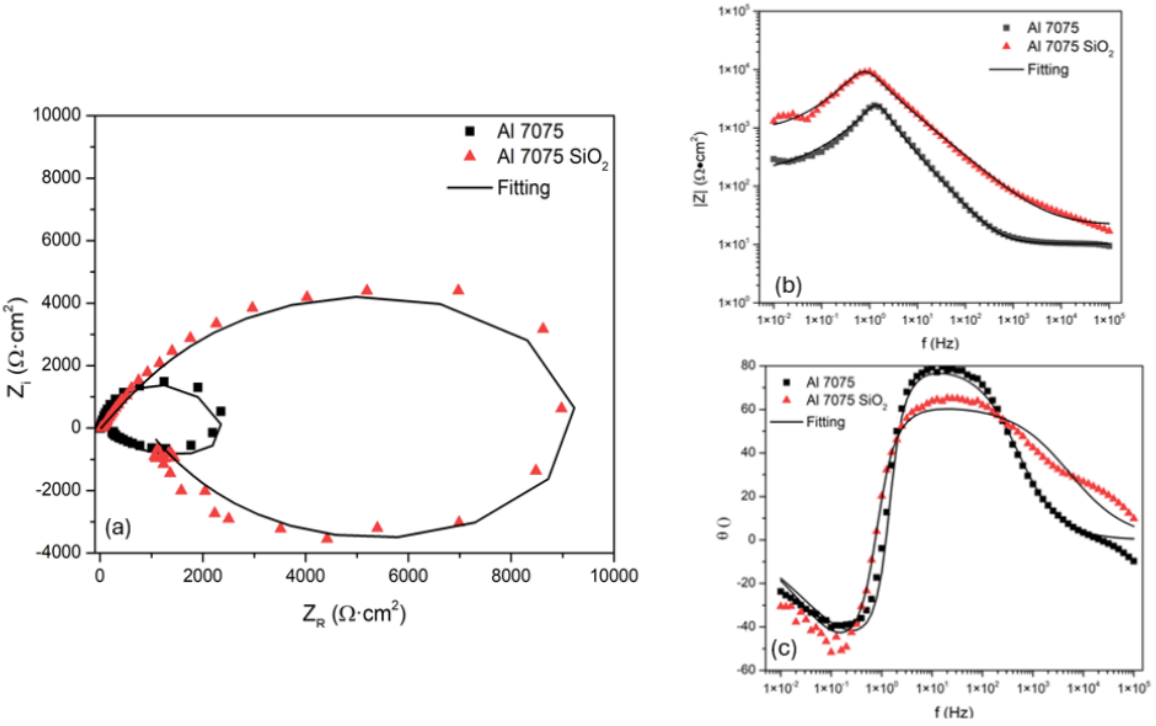

Figure 4. EIS of samples when is exposed to NaCl (a) Nyquist diagram, (b) Bode plot of frequency vs |Z|, and (c) frequency and phase angle.

Figure 5 shows the behavior when samples are exposed to H_2SO_4. Figure 5(a) shows the Nyquist diagram, supported by Figure 5(b) of absolute impedance. In both graphics, it is notable how the behavior of Al 7075 and Al 7075 SiO2 presented the same characteristics at high frequencies; however, at middle and low frequencies, the corrosion resistance of Al 7075 is higher than that of the sample coated. It is because the H_2SO_4 generates an oxide layer in aluminum that protects the material. Also, the electrolyte can be very aggressive for the superhydrophobic. The IE is negative due to the lower resistance presented by the material. N values of the first layer are 0.92 and 0.93; therefore, the behavior is capacitive, and the distribution of charge is nearly homogeneous. On the second layer, the values are negative, indicating an adsorption process that occurs on the surface. The adsorption process is more homogeneous for the uncoated sample; therefore, the n value is -0.87.

 doi:10.20944/preprints202508.1927.v1

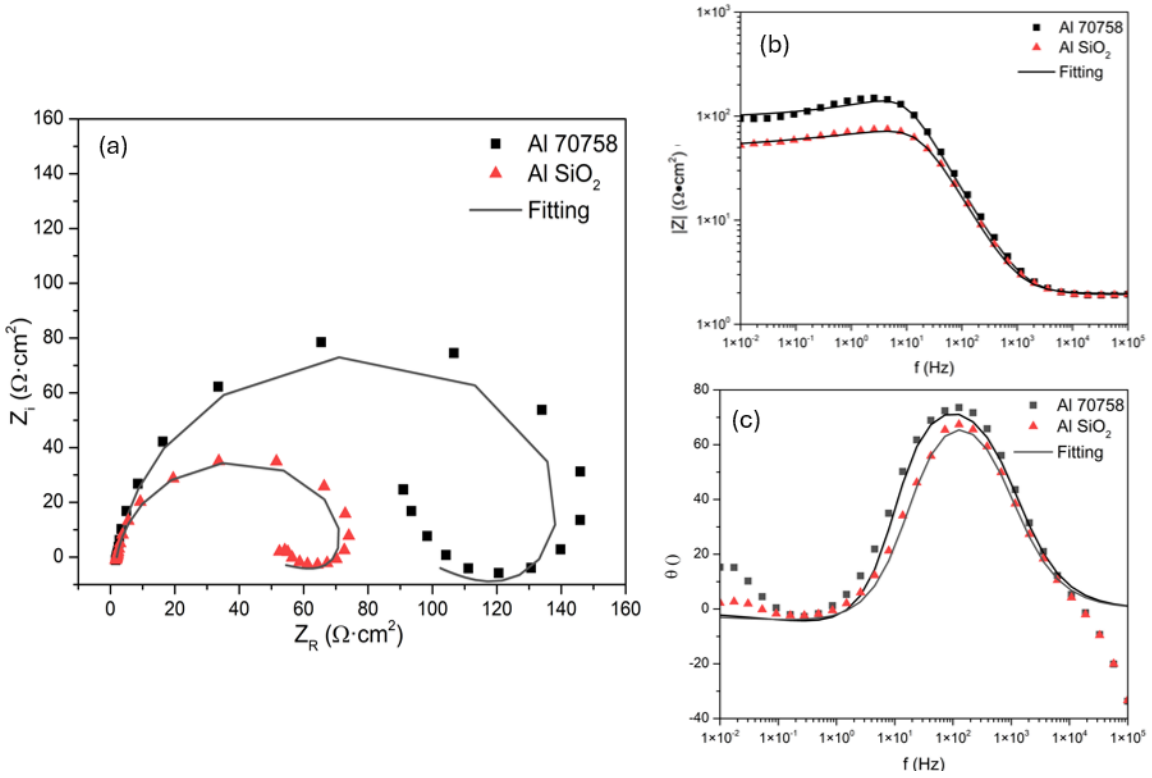

Figure 5. EIS of samples when they is exposed to H_2SO_4 (a) Nyquist diagram, (b) Bode plot of frequency vs |Z|, and (c) frequency and phase angle.

Figure 6 shows the equivalent circuits for the sample uncoated (a) and the sample with inhibitor (b). The behavior is the same; the difference is that the first layer is related to the oxide generated by the interaction of the electrolyte with the metal for Al 7075. In Figure 6(b), the first layer is related to the resistance of the inhibitor. The behavior of CPE from the second layer is associated with an inductor by the negative values of n.

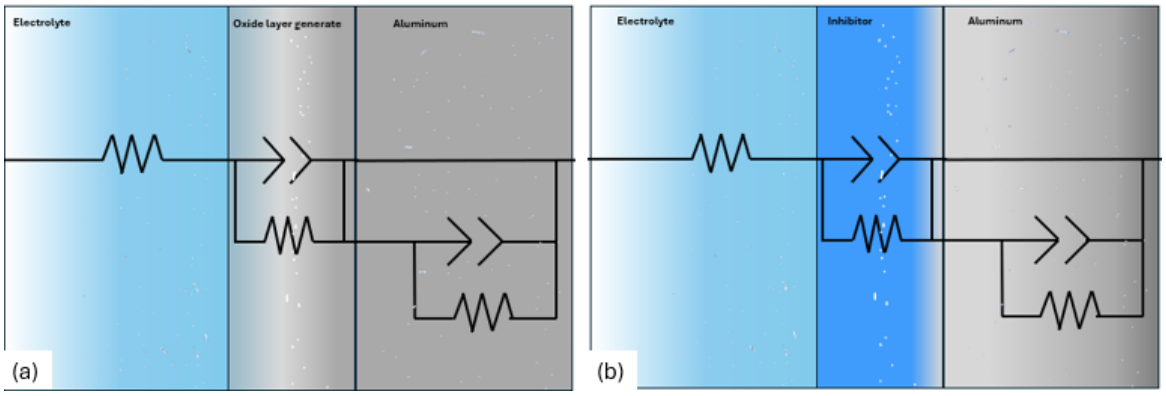

Figure 6. Equivalent circuits for (a) Al 7075 and (b) Al 7075 SiO_2.

 doi:10.20944/preprints202508.1927.v1

Table 2. Parameters obtained by EIS.

Sample	Rs (Ω·cm²)	CPE1-T (F/cm²)	n	R_{ct} (Ω·cm²)	CPE2-T (F/cm²)	n	R_C (Ω·cm²)	IE (%)
NaCl								
Al 7075	21.3	3.6×10^{-5}	0.68698	874	3.42×10^{-4}	-0.70	1.04×10^{3}	-
Al 7075 SiO_2	10.35	6.6×10^{-5}	0.9036	177	2.09×10^{-3}	-0.68	1.01×10^{4}	81.37
H_2SO_4								
Al 7075	1.928	1.1×10^{-4}	0.9386	99	0.066	-0.87	52.95	-
Al 7075 SiO_2	1.985	1.5×10^{-4}	0.92533	52	0.11	-0.76	22.91	-102

3.4. SEM After Corrosion Test

Figure 7 shows the samples after the corrosion test in NaCl. Figures 7(a-b) show the uncoated Al 7075, where the distribution of oxide and corrosion residuals is not homogeneous; therefore, the values of n are not 1 in EIS. Also, this figure supports the results obtained by CPP, where the type of corrosion was localized, due to the localization of corrosion in preference zones. Something similar occurs with Figure 7(c-d), where the superhydrophobic presented degradation in the cracked zones. The corrosion attacks the cracking zones preferentially, generating a localized attack.

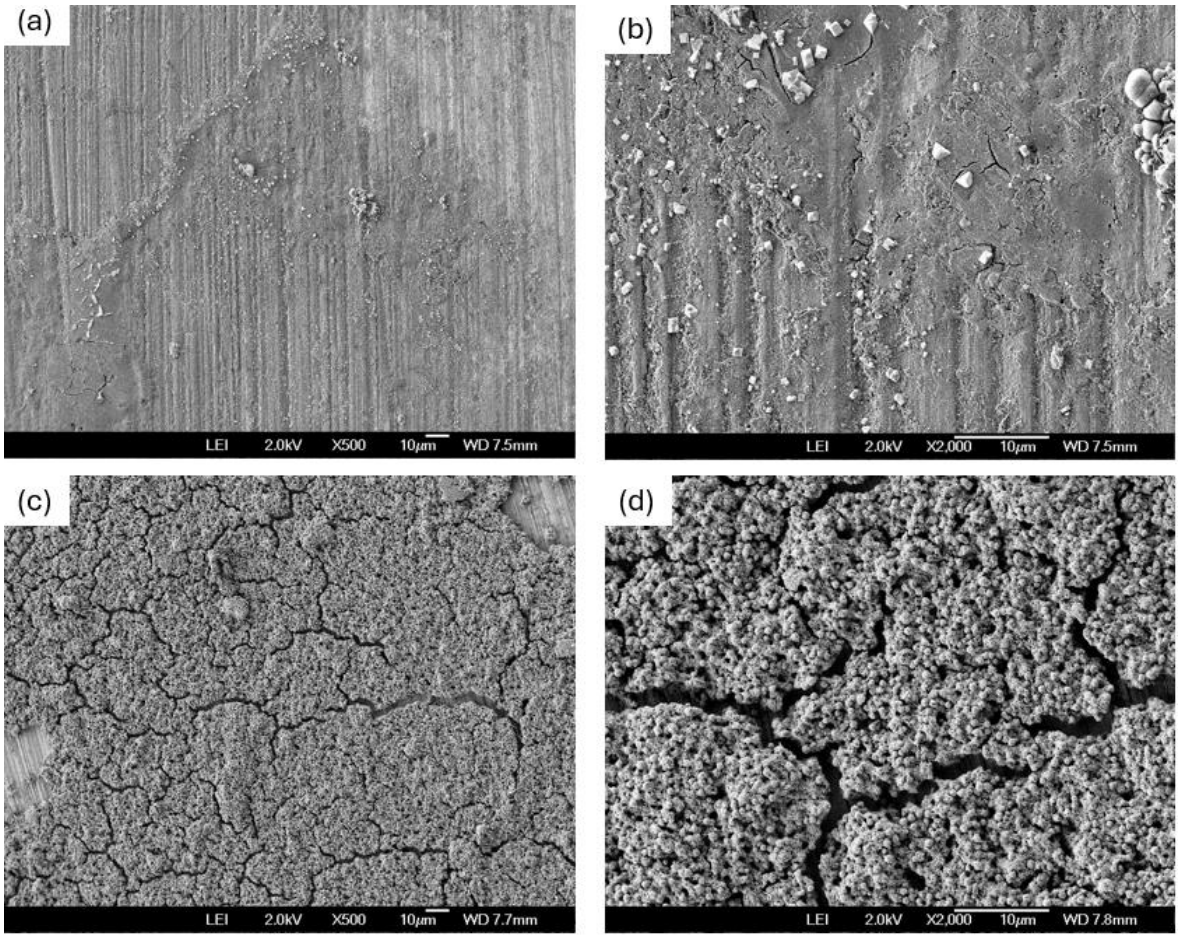

Figure 7. SEM images of aluminum uncoated (a-b) and aluminum with SiO_2 inhibitor (c-d) at 500 and 2000X after being exposed to NaCl.

Figure 8 shows the samples after the corrosion test on H_2SO_4. Figures 8(a-b) show that the distribution of attack is more homogeneous; however, the corrosion residuals are more concentrated

 doi:10.20944/preprints202508.1927.v1

in some zones. Figure 8(c-d) shows how dissolution begins in the cracking zones as a localized process, resulting in a uniform dissolution with the generation of an oxide layer. The formed oxide layer shows areas of cracking, suggesting that corrosion becomes uniform over time. Therefore, the CPP results confirm that uniform corrosion is taking place on the surface.

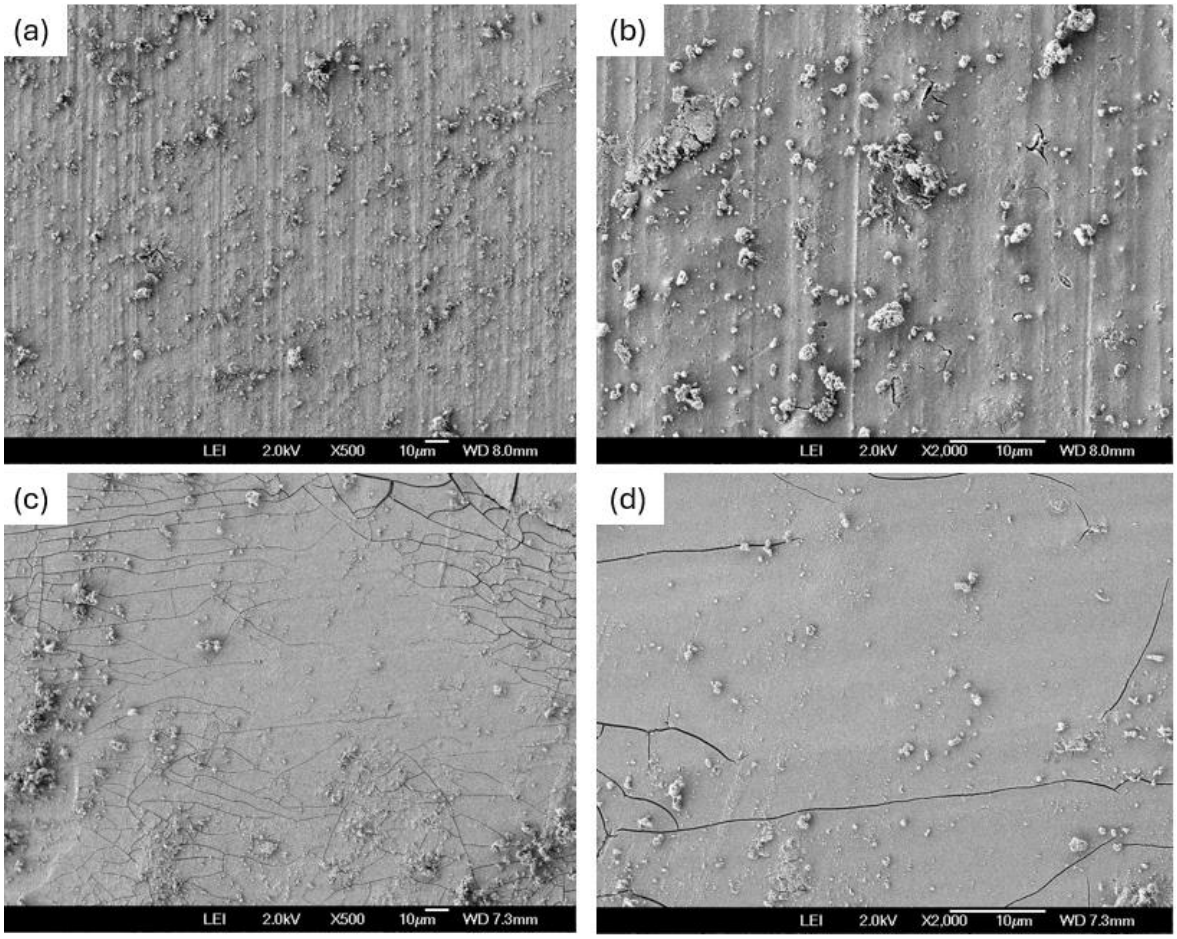

Figure 8. SEM images of aluminum uncoated (a-b) and aluminum with SiO_2 inhibitor (c-d) at 500 and 2000X after being exposed to H_2SO_4.

4. Discussion

Water droplets are retained due to the hierarchical structure of the coating. Designing such hierarchical features and modifying surface roughness are essential steps in developing an effective hydrophobic layer. In the case of superhydrophobic coatings, the presence of multiscale roughness enhances water repellency, durability, and self-cleaning properties. Morphological and structural analyses confirmed that the coating's hierarchical architecture, formed by nano- and microscale particles, contributes to its roughness and superhydrophobic behavior [33,34].

The anodic reaction in aluminum involves the transformation of Al^{3+} into ions, as represented in the following equation.

$$Al_{(s)} \rightarrow Al^{3+}_{(aq)} + 3e^{-} \quad (3)$$

In NaCl composites, the chloride ion (Cl^-) plays a key role in the electrochemical corrosion of the material. The following equation illustrates the reaction between Cl^- and aluminum. These reactions promote active oxidation; as oxygen diffuses through the surface, the resulting corrosion products become porous and fail to maintain passivation. Consequently, localized attacks occur, and pitting develops in the ferrite regions, as Cl^- ions preferentially penetrate those zones [35,36]. Chloride ions

 doi:10.20944/preprints202508.1927.v1

hinder the formation of a stable oxide film on the metal surface by destabilizing the protective layer and creating weak spots that expose the substrate to localized corrosion, entering as interstitial ions.

$$Al^{3+}{}_{(aq)} + 3Cl^{-}{}_{(aq)} \rightarrow AlCl_3 \quad (4)$$

Although aluminum spontaneously generates a passive layer, it often shows inhomogeneities. The presence of Cl^- further disrupts its stability [37]. According to different research, certain ions pose greater risks to specific alloys, with Cl^- being particularly aggressive. While H_2SO_4 may induce higher dissolution, chloride ions cause more long-term damage by penetrating and dissolving the passive film through diffusion. As a result, the oxide layer formed by NaCl in Al-7075 exhibits pitting corrosion due to the instability generated by Cl^- at the surface.

This susceptibility of aluminum to chloride ions reinforces the earlier statement that Cl^- governs the behavior of the passive film in NaCl electrolytes, preventing its uniform formation [37–39]. Additionally, hydroxide reactions further intensify degradation in various materials, as aluminum hydroxide is produced according to the following equation.

$$Al^{3+}{}_{(aq)} + 3OH^{-}{}_{(aq)} \rightarrow Al(OH)_{3(s)} \quad (51)$$

In contrast, the reaction of H_2SO_4 can lead to the formation of a stable oxide layer; however, due to its aggressiveness, the oxide may sometimes become unstable and dissolve in the acidic medium. Under such conditions, aluminum undergoes dissolution driven by the electrolyte's aggressiveness, producing hydrogen gas and causing a shift in the electrolyte's pH [40–43]. The corrosion behavior of Al-7075 with inhibitors in H_2SO_4 can present a uniform corrosion mechanism within the acidic environment. The surface of the specimen was almost entirely covered with corrosion, and the presence of consistent cracks and depressions confirmed the uniform nature of the process. Furthermore, immersion in H_2SO_4 leads to greater material degradation, reflected in lower hardness values compared to specimens exposed to NaCl solution [44].

Figure 8 shows the corrosion diagram when Al 7075 SiO_2 is exposed to the different electrolytes. Figure 8(a) shows the behavior when it is exposed to NaCl. The Cl^- ions attack in the cracking zones, with the reaction of the oxygen generating the corrosion residual presented in equation 4. The Cl^- ions attack on the cracking zones, propitiating the dissolution of the superhydrophobic. The zone where the ions penetrate an oxide layer is generated; therefore, the corrosion type that is presented in the sample is localized. However, it is important to check that the results show a decrease in corrosion rate, with a magnitude of ×10-5 A/cm2 for the coated sample and ×10-4 A/cm2 for the uncoated sample, indicating that the inhibitor achieves its function in NaCl.

When a sample is exposed to H2SO4, the corrosion mechanism is similar. The corrosive ions attack the cracking areas. The difference is that the H_2SO_4 is more aggressive and dissolves SiO_2. After that, the oxide layer is generated. Therefore, Al7075 presented a higher corrosion resistance in H2SO4 when evaluated by EIS. The oxide layer created by exposure to this medium is more resistive. However, the results obtained by CPP of the Al 7075 SiO2 showed a lower corrosion rate, due to the corrosion inhibitor delaying the corrosion. In EIS, the results are different because this technique evaluates the oxide layer generated, and the perturbation generated by EIS is lower than that generated by CPP. Therefore, the oxide layer generated by CPP can be dissolved more easily. The oxide layer generated in Al 7075 by H_2SO_4 is not unstable. Figure 7 shows it how the oxide layer is non-homogeneous.

 doi:10.20944/preprints202508.1927.v1

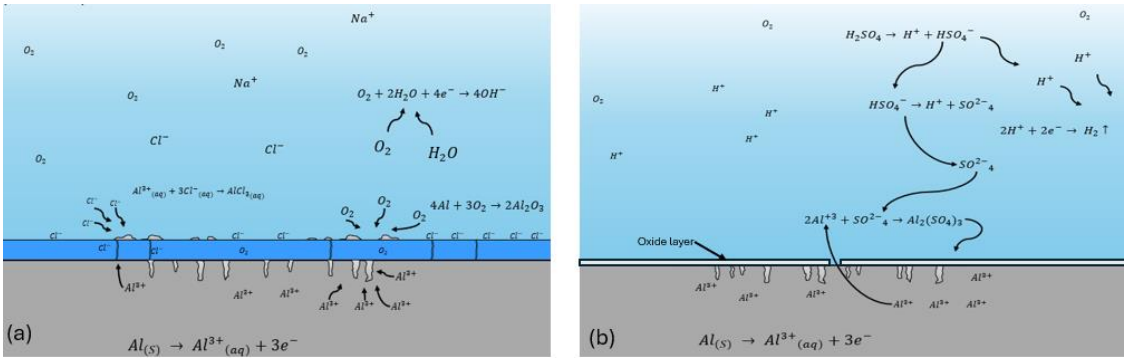

Figure 8. Diagram of corrosion mechanisms in each electrolyte for Al 7075 SiO_2. Figure (a) represents the corrosion mechanism when it is exposed to (a) NaCl and (b) H_2SO_4.

The results obtained by CPP in H_2SO_4 did not present a passivation zone. An anodic breach is occurring, indicating a current demand. However, the current demand decreases in comparison with the CPP when samples are exposed to NaCl when the activation zone is pure, so the anodic breach of samples in H_2SO_4 presented a behavior near to pseudopasivation, for that reason, a layer of oxide was generated on the surface.

The values obtained by EIS showed n's values of 0.68 for Al 7075 indicating that surface is not homogenous, the second layer is of -0.70, indicating that the absorption process is occurring in the surface, however, that adsorption continue being heterogenous, the same behavior is for Al 7075 SiO_2 in the second layer, where a heterogenous adsorption process occurs on surface due to n value of 0.68, however the first layer obtained a value of 0.90 in n, indicating that the superhydrophobic coating is well distributed; however it is not perfect, the cracking zones from figure 1 cased the 0.90 value [45–49].

The value of Rct is the value associated with the inhibitor resistance. The resistance of the coating in NaCl is 177 Ω·cm2, and in H2SO4, it is 52 Ω·cm2. This indicates a higher efficiency of coating in NaCl than in H_2SO_4. It's recommended to use this coating in NaCl. In H2SO4, the coating does not protect the material in the same way as in NaCl.

5. Conclusions

- The coating of SiO_2 presented a hierarchical structure, with a heterogeneous distribution, nearly homogeneous; however, it presented crack zones that helped as a corrosion concentrator.
- Samples coated with superhydrophobic coatings showed a reduction in corrosion rate obtained by CPP, indicating that the coating protects the material.
- The Al 7075 coated with SiO2 presented localized corrosion when exposed to NaCl. Cl^- ions attack on the cracking zone. On the other hand, the H_2SO_4 coating presented a uniform corrosion due to the dissolution of the coating in this medium.
- The inhibitor efficiency in NaCl is 81%, indicating higher corrosion resistance. Also, the R_{ct} value of Al 7075 coated by SiO_2 exposed to H_2SO_4 is 70% lower than the R_{ct} in NaCl; therefore, this coating can be employed in marine atmospheres.
- The behavior of Al 7075 coated with SiO_2 presented an inductive behavior, indicating that adsorption phenomena are occurring on the surface. This is the natural aluminum behavior, and the coating did not change it.

Author Contributions: Conceptualization J.M.J.M and D.C.M.; methodology J.M.J.M, D.C.M, M.G.C.R, B.S.S.; formal analysis, J.M.J.M, L.E.V.N, M.G.C.R, A.A.L.I and B.S.S; investigation, L.E.V.N, J.G.S.E, A.D.O and J.S.A.C.; data curation, J.M.J.M, L.E.V.N, J.G.S.E AND A.D.O.; writing—original draft preparation, J.M.J.M, D.C.M and J.S.A.C.; writing—review and editing, J.M.J.M, L.E.A.M; supervision, J.M.J.M.; funding acquisition J.M.J.M, J.G.S.E, L.E.A.M and A.D.O All authors have read and agreed to the published version of the manuscript." Please

 doi:10.20944/preprints202508.1927.v1

turn to the CRediT taxonomy for the term explanation. Authorship must be limited to those who have contributed substantially to the work reported.

Funding: This research was funded by by Universidad Autónoma de Aguascalientes".

References

1. Liu, M.; Guo, Y.; Wang, J.; Yergin, M. Corrosion Avoidance in Lightweight Materials for Automotive Applications. npj Mater. Degrad. 2018 21 2018, 2, 1–4, doi:10.1038/s41529-018-0045-2.
2. Vukkum, V.B.; Christudasjustus, J.; Darwish, A.A.; Storck, S.M.; Gupta, R.K. Enhanced Corrosion Resistance of Additively Manufactured Stainless Steel by Modification of Feedstock. npj Mater. Degrad. 2022 61 2022, 6, 1–11, doi:10.1038/s41529-021-00215-z.
3. Shin, B.H.; Park, J.; Jeon, J.; Heo, S. bo; Chung, W. Effect of Cooling Rate after Heat Treatment on Pitting Corrosion of Super Duplex Stainless Steel UNS S 32750. Anti-Corrosion Methods Mater. 2018, 65, 492–498, doi:10.1108/ACMM-05-2018-1939/FULL/XML.
4. Kumar, A.; Singh, J. OVERVIEW ON CORROSION IN AUTOMOTIVE INDUSTRY AND THERMAL POWER PLANT. Proc. Eng. Sci. 2022, 4, 13–22, doi:10.24874/PES04.01.003.
5. Yin, Z.Z.; Qi, W.C.; Zeng, R.C.; Chen, X.B.; Gu, C.D.; Guan, S.K.; Zheng, Y.F. Advances in Coatings on Biodegradable Magnesium Alloys. J. Magnes. Alloy. 2020, 8, 42–65, doi:10.1016/J.JMA.2019.09.008.
6. Yamauchi, N.; Ueda, N.; Okamoto, A.; Sone, T.; Tsujikawa, M.; Oki, S. DLC Coating on Mg–Li Alloy. Surf. Coatings Technol. 2007, 201, 4913–4918, doi:10.1016/J.SURFCOAT.2006.07.080.
7. Sukiman, N.L.; Zhou, X.; Birbilis, N.; Hughes, A.E.; Mol, J.M.C.; Garcia, S.J.; Zhou, X.; Thompson, G.E.; Sukiman, N.L.; Zhou, X.; et al. Durability and Corrosion of Aluminium and Its Alloys: Overview, Property Space, Techniques and Developments. Alum. Alloy. - New Trends Fabr. Appl. 2012, doi:10.5772/53752.
8. Hussain, C.M.; Verma, C.; Aslam, J.; Aslam, R.; Zehra, S. Handbook of Corrosion Engineering: Modern Theory, Fundamentals and Practical Applications. Handb. Corros. Eng. Mod. Theory, Fundam. Pract. Appl. 2023, 1–459, doi:10.1016/C2021-0-02205-7.
9. Kadhim, A.; Al-Amiery, A.A.; Alazawi, R.; Al-Ghezi, M.K.S.; Abass, R.H. Corrosion Inhibitors. A Review. Int. J. Corros. Scale Inhib. 2021, 10, 54–67, doi:10.17675/2305-6894-2021-10-1-3.
10. Sopha, H.; Norikawa, Y.; Motola, M.; Hromadko, L.; Rodriguez-Pereira, J.; Cerny, J.; Nohira, T.; Yasuda, K.; Macak, J.M. Anodization of Electrodeposited Titanium Films towards TiO2 Nanotube Layers. Electrochem. commun. 2020, 118, 106788, doi:10.1016/J.ELECOM.2020.106788.
11. Islam, M.; Azhar, M.R.; Fredj, N.; Burleigh, T.D.; Oloyede, O.R.; Almajid, A.A.; Ismat Shah, S. Influence of SiO2 Nanoparticles on Hardness and Corrosion Resistance of Electroless Ni–P Coatings. Surf. Coatings Technol. 2015, 261, 141–148, doi:10.1016/J.SURFCOAT.2014.11.044.
12. Kasturibai, S.; Kalaignan, G.P. Physical and Electrochemical Characterizations of Ni-SiO2 Nanocomposite Coatings. Ionics (Kiel). 2013, 19, 763–770, doi:10.1007/S11581-012-0810-0/METRICS.
13. Sinha Ray, S.; Okamoto, M. Polymer/Layered Silicate Nanocomposites: A Review from Preparation to Processing. Prog. Polym. Sci. 2003, 28, 1539–1641, doi:10.1016/J.PROGPOLYMSCI.2003.08.002.
14. Ruhi, G.; Modi, O.P.; Sinha, A.S.K.; Singh, I.B. Effect of Sintering Temperatures on Corrosion and Wear Properties of Sol–Gel Alumina Coatings on Surface Pre-Treated Mild Steel. Corros. Sci. 2008, 50, 639–649, doi:10.1016/J.CORSCI.2007.10.002.
15. Hosseini, M.; Karapanagiotis, I. Materials with Extreme Wetting Properties: Methods and Emerging Industrial Applications. Mater. with Extrem. Wetting Prop. Methods Emerg. Ind. Appl. 2021, 1–370, doi:10.1007/978-3-030-59565-4/COVER.
16. Sajadi, G.S.; Ali Hosseini, S.M.; Saheb, V.; Shahidi-Zandi, M. Using of Asymmetric Cell to Monitor Corrosion Performance of 304 Austenitic Stainless Steel by Electrochemical Noise Method. J. Mater. Res. Technol. 2023, 22, 107–125, doi:10.1016/J.JMRT.2022.11.082.
17. Ribeiro, T.; Baleizão, C.; Farinha, J.P.S. Functional Films from Silica/Polymer Nanoparticles. Mater. 2014, Vol. 7, Pages 3881-3900 2014, 7, 3881–3900, doi:10.3390/MA7053881.

 doi:10.20944/preprints202508.1927.v1

18. Yan, Y.L.; Cai, Y.X.; Liu, X.C.; Ma, G.W.; Lv, W.; Wang, M.X. Hydrophobic Modification on the Surface of SiO2Nanoparticle: Wettability Control. Langmuir 2020, 36, 14924–14932, doi:10.1021/ACS.LANGMUIR.0C02118/SUPPL_FILE/LA0C02118_SI_001.PDF.
19. Heinz, H.; Pramanik, C.; Heinz, O.; Ding, Y.; Mishra, R.K.; Marchon, D.; Flatt, R.J.; Estrela-Lopis, I.; Llop, J.; Moya, S.; et al. Nanoparticle Decoration with Surfactants: Molecular Interactions, Assembly, and Applications. Surf. Sci. Rep. 2017, 72, 1–58, doi:10.1016/J.SURFREP.2017.02.001.
20. Chen, H.; Fan, H.; Su, N.; Hong, R.; Lu, X. Highly Hydrophobic Polyaniline Nanoparticles for Anti-Corrosion Epoxy Coatings. Chem. Eng. J. 2021, 420, 130540, doi:10.1016/J.CEJ.2021.130540.
21. Fuji, M.; Takei, T.; Watanabe, T.; Chikazawa, M. Wettability of Fine Silica Powder Surfaces Modified with Several Normal Alcohols. Colloids Surfaces A Physicochem. Eng. Asp. 1999, 154, 13–24, doi:10.1016/S0927-7757(98)00905-4.
22. Al-Haidary, J.T.; Haddad, J.S.; Alfaqs, F.A.; Zayadin, F.F. Susceptibility of Aluminum Alloy 7075 T6 to Stress Corrosion Cracking. SAE Int. J. Mater. Manuf. 2020, 14, 195–201, doi:10.4271/05-14-02-0013.
23. Kairy, S.K.; Turk, S.; Birbilis, N.; Shekhter, A. The Role of Microstructure and Microchemistry on Intergranular Corrosion of Aluminium Alloy AA7085-T7452. Corros. Sci. 2018, 143, 414–427, doi:10.1016/J.CORSCI.2018.08.033.
24. Cheng, X.; Li, X.; Yang, L.; Du, C. Corrosion Resistance of 316L Stainless Steel in Acetic Acid by EIS and Mott-Schottky. J. Wuhan Univ. Technol. Mater. Sci. Ed. 2008, 23, 574–578, doi:10.1007/S11595-006-4574-0/METRICS.
25. Xiong, Y.; Robson, J.D.; Yao, Y.; Zhong, X.; Guarracino, F.; Bendo, A.; Jin, Z.; Hashimoto, T.; Liu, X.; Curioni, M. Effects of Heat Treatments on the Microstructure and Localized Corrosion Behaviors of AA7075 Aluminum Alloy. Corros. Sci. 2023, 221, 111361, doi:10.1016/J.CORSCI.2023.111361.
26. Gupta, R.; Verma, R.; Kango, S.; Constantin, A.; Kharia, P.; Saini, R.; Kudapa, V.K.; Mittal, A.; Prakash, J.; Chamoli, P. A Critical Review on Recent Progress, Open Challenges, and Applications of Corrosion-Resistant Superhydrophobic Coating. Mater. Today Commun. 2023, 34, 105201, doi:10.1016/J.MTCOMM.2022.105201.
27. Qiao, M.; Ji, G.; Lu, Y.; Zhang, B. Sustainable Corrosion-Resistant Superhydrophobic Composite Coating with Strengthened Robustness. J. Ind. Eng. Chem. 2023, 121, 215–227, doi:10.1016/J.JIEC.2023.01.025.
28. Mamgain, H.P.; Pati, P.R.; Samanta, K.K.; Brajpuriya, R.; Gupta, R.; Pandey, J.K.; Giri, J.; Sathish, T.; Kanan, M. A Review on Bio-Inspired Corrosion Resistant Superhydrophobic Coating on Copper Substrate: Recent Advances, Mechanisms, Constraints, and Future Prospects. Results Eng. 2025, 25, 103868, doi:10.1016/J.RINENG.2024.103868.
29. Tian, Y.; Li, H.; Wang, M.; Yang, C.; Yang, Z.; Liu, X. Insights into the Stability of Fluorinated Superhydrophobic Coating in Different Corrosive Solutions. Prog. Org. Coatings 2021, 151, 106043, doi:10.1016/J.PORGCOAT.2020.106043.
30. Chen, X.; Wang, P.; Zhang, D.; Ou, J. Effect of Surface Nanostructure on Enhanced Atmospheric Corrosion Resistance of a Superhydrophobic Surface. Colloids Surfaces A Physicochem. Eng. Asp. 2022, 647, 129058, doi:10.1016/J.COLSURFA.2022.129058.
31. ASTM Standard G61-86 "Standard Test Method for Conducting Cyclic Potentiodynamic Polarization Measurements for Localized Corrosion Susceptibility of Iron, Nickel or Cobalt Based Aalloys"; 2010; Vol. 86;.
32. Liu, T.; Chen, S.; Cheng, S.; Tian, J.; Chang, X.; Yin, Y. Corrosion Behavior of Superhydrophobic Surface on Copper in Seawater. Electrochim. Acta 2007, 52, 8003–8007, doi:10.1016/J.ELECTACTA.2007.06.072.
33. Jin, M.; Xing, Q.; Chen, Z.; Jin, M.; Xing, Q.; Chen, Z. A Review: Natural Superhydrophobic Surfaces and Applications. J. Biomater. Nanobiotechnol. 2020, 11, 110–149, doi:10.4236/JBNB.2020.112008.
34. Feng, B.L.; Li, S.; Li, Y.; Li, H.; Zhang, L.; Zhai, J.; Song, Y.; Liu, B.; Jiang, L. Superhydrophobic Surfaces: From Natural to Artificial. Adv. Mater. 2002, 1857–1860.
35. Sharma, A.; McQuillan, A.J.; A Sharma, L.; Waddell, J.N.; Shibata, Y.; Duncan, W.J. Spark Anodization of Titanium–Zirconium Alloy: Surface Characterization and Bioactivity Assessment. J. Mater. Sci. Mater. Med. 2015, 26, 1–11, doi:10.1007/S10856-015-5555-7/FIGURES/5.

 doi:10.20944/preprints202508.1927.v1

36. Shibaeva, T. V.; Laurinavichyute, V.K.; Tsirlina, G.A.; Arsenkin, A.M.; Grigorovich, K. V. The Effect of Microstructure and Non-Metallic Inclusions on Corrosion Behavior of Low Carbon Steel in Chloride Containing Solutions. Corros. Sci. 2014, 80, 299–308, doi:10.1016/J.CORSCI.2013.11.038.
37. Wang, Z.B.; Hu, H.X.; Zheng, Y.G. Synergistic Effects of Fluoride and Chloride on General Corrosion Behavior of AISI 316 Stainless Steel and Pure Titanium in H2SO4 Solutions. Corros. Sci. 2018, 130, 203–217, doi:10.1016/J.CORSCI.2017.10.028.
38. Feizi Mohazzab, B.; Jaleh, B.; Kakuee, O.; Fattah-alhosseini, A. Formation of Titanium Carbide on the Titanium Surface Using Laser Ablation in N-Heptane and Investigating Its Corrosion Resistance. Appl. Surf. Sci. 2019, 478, 623–635, doi:10.1016/J.APSUSC.2019.01.259.
39. Engelhardt, G.R.; Macdonald, D.D. Monte-Carlo Simulation of Pitting Corrosion with a Deterministic Model for Repassivation. J. Electrochem. Soc. 2020, 167, 013540, doi:10.1149/1945-7111/AB67A0.
40. Vasilescu, C.; Drob, S.I.; Osiceanu, P.; Calderon-Moreno, J.M.; Drob, P.; Vasilescu, E. Characterisation of Passive Film and Corrosion Behaviour of a New Ti-Ta-Zr Alloy in Artificial Oral Media: In Time Influence of PH and Fluoride Ion Content. Mater. Corros. 2015, 66, 971–981, doi:10.1002/MACO.201408025.
41. Castany, P.; Gordin, D.M.; Drob, S.I.; Vasilescu, C.; Mitran, V.; Cimpean, A.; Gloriant, T. Deformation Mechanisms and Biocompatibility of the Superelastic Ti–23Nb–0.7Ta–2Zr–0.5N Alloy. Shape Mem. Superelasticity 2016, 2, 18–28, doi:10.1007/S40830-016-0057-0/FIGURES/7.
42. Liu, C.; Bi, Q.; Leyland, A.; Matthews, A. An Electrochemical Impedance Spectroscopy Study of the Corrosion Behaviour of PVD Coated Steels in 0.5 N NaCl Aqueous Solution: Part II.: EIS Interpretation of Corrosion Behaviour. Corros. Sci. 2003, 45, 1257–1273, doi:10.1016/S0010-938X(02)00214-7.
43. Wicaksono, A.B.; Sutanto, H.; Ruslan, W. Effects of Immersion in the NaCl and H2SO4 Solutions on the Corrosion Rate, Microstructure, and Hardness of Stainless Steel 316L. Res. Eng. Struct. Mat 2023, 9, 1153–1168, doi:10.17515/resm2023.695ma0220.
44. Wongpanya, P.; Wongpinij, T.; Photongkam, P.; Siritapetawee, J. Improvement in Corrosion Resistance of 316L Stainless Steel in Simulated Body Fluid Mixed with Antiplatelet Drugs by Coating with Ti-Doped DLC Films for Application in Biomaterials. Corros. Sci. 2022, 208, 110611, doi:10.1016/J.CORSCI.2022.110611.
45. Liu, X.; Wang, P.; Zhang, D. Facile Fabrication of High-Aspect-Ratio Superhydrophobic Surface with Self-Propelled Droplet Jumping Behavior for Atmospheric Corrosion Protection. Appl. Surf. Sci. 2021, 555, 149549, doi:10.1016/J.APSUSC.2021.149549.
46. Li, X.; Yan, J.; Yu, T.; Zhang, B. Versatile Nonfluorinated Superhydrophobic Coating with Self-Cleaning, Anti-Fouling, Anti-Corrosion and Mechanical Stability. Colloids Surfaces A Physicochem. Eng. Asp. 2022, 642, 128701, doi:10.1016/J.COLSURFA.2022.128701.
47. Zhang, H.; Hao, L.; Wang, J.; Zhang, S.; Zhang, C.; Ke, W. EIS Evaluation on the Degradation Behavior of Rust-Preventive Oil Coating Exposure to NaCl Electrolyte. Electrochim. Acta 2024, 492, 144359, doi:10.1016/J.ELECTACTA.2024.144359.
48. Chávez-Díaz, M.P.; Luna-Sánchez, R.M.; Vazquez-Arenas, J.; Lartundo-Rojas, L.; Hallen, J.M.; Cabrera-Sierra, R. XPS and EIS Studies to Account for the Passive Behavior of the Alloy Ti-6Al-4V in Hank's Solution. J. Solid State Electrochem. 2019, 23, 3187–3196, doi:10.1007/S10008-019-04368-5/METRICS.
49. Macdonald, J.R. Generalizations of '"Universal Dielectric Response"' and a General Distribution-of-activation-energies Model for Dielectric and Conducting Systems. J. Appl. Phys. 1985, 58, 1971–1978, doi:10.1063/1.336004.